



This is a repository copy of *Wheat root system architecture and soil moisture distribution in an aggregated soil using neutron computed tomography*.

White Rose Research Online URL for this paper:
<http://eprints.whiterose.ac.uk/152696/>

Version: Accepted Version

Article:

Mawodza, T., Burca, G., Casson, S. et al. (1 more author) (2020) Wheat root system architecture and soil moisture distribution in an aggregated soil using neutron computed tomography. *Geoderma*, 359. ISSN 0016-7061

<https://doi.org/10.1016/j.geoderma.2019.113988>

Article available under the terms of the CC-BY-NC-ND licence
(<https://creativecommons.org/licenses/by-nc-nd/4.0/>).

Reuse

This article is distributed under the terms of the Creative Commons Attribution-NonCommercial-NoDerivs (CC BY-NC-ND) licence. This licence only allows you to download this work and share it with others as long as you credit the authors, but you can't change the article in any way or use it commercially. More information and the full terms of the licence here: <https://creativecommons.org/licenses/>

Takedown

If you consider content in White Rose Research Online to be in breach of UK law, please notify us by emailing eprints@whiterose.ac.uk including the URL of the record and the reason for the withdrawal request.

1 **Wheat Root System Architecture and Soil Moisture Distribution in an Aggregated Soil**
2 **using Neutron Computed Tomography.**

3 Tinashe Mawodza^{1*}, Genoveva Burca², Stuart Casson¹, Manoj Menon³

4 ¹Department of Molecular Biology and Biotechnology, The University of Sheffield, Western
5 Bank, Sheffield S10 2TN, United Kingdom

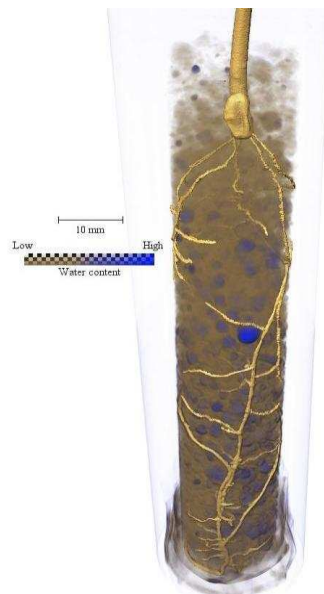
6 ²STFC, Rutherford Appleton Laboratory, ISIS Facility, Harwell, OX11 0QX, UK

7 ³Department of Geography, The University of Sheffield, 9 Northumberland Rd, Sheffield S10
8 2TN

9 * Corresponding author E-mail address: tmawodza1@sheffield.ac.uk

10 Non-invasive techniques are essential to deepen our understanding of root-soil interactions in
11 situ. Neutron computed tomography (NCT) is an example of such techniques that have been
12 successfully used to study these interactions in high resolution. Many of the studies using
13 NCT however, have invariably focused on lupine plants and thus there is limited information
14 available on other more commercially important staple crop plants such as wheat and rice.
15 Also considering the high neutron sensitivity to hydrogen (e.g. water in roots or soil organic
16 matter), nearly all previous in-situ NCT studies have used a relatively homogeneous porous
17 media such as sand, low in soil organic matter and free from soil aggregates, to obtain high-
18 quality images. However to expand the scope of the use of NCT to other more commercially
19 important crops and in less homogenous soils, in this study we focused on wheat root growth
20 in a soil that contained a considerable amount of soil organic matter (SOM) and different
21 sized aggregates. As such, the main aims of this research were (1) to unravel wheat (*Triticum*
22 *aestivum* cv. Fielder) root system architecture (RSA) when grown in an aggregated sandy
23 loam soil (<4 mm) with 4% SOM content, (2) Map in 3D, soil water distribution after a brief
24 drying period and (3) to understand how the root system interacts with soil moisture

25 distribution brought about by soil structural heterogeneity. To achieve these, wheat seedlings
26 were grown for 13-days in aluminium tubes (100 mm height and 18 mm diameter) packed
27 with soil and imaged for the first time at the IMAT neutron beamline (in the Rutherford
28 Appleton Laboratory, UK). To the best of our knowledge, this is also the first study to use
29 NCT to study wheat root architectural development. Our study proved that NCT can
30 successfully be used to reveal wheat RSA in a heterogeneous aggregated soils with moderate
31 amounts of SOM. Lateral root growth within the soil column was increased in regions with
32 increased finer soil separates. NCT was also able to successfully map water distribution in a
33 3D and we show that large macro-aggregates preferentially retained relatively higher soil
34 moisture in comparison to the smaller soil separates within our samples (Fig. 1). This
35 highlights the importance large macro-aggregates in sustainable soil management as they
36 may be able to provide plants water during periodic dry spells. More in situ investigations are
37 required to further understand the impact of different aggregate sizes on RSA and water
38 uptake.



39
40 Figure 1: NCT image of a 13-day old wheat seedling root growing in an aggregated sandy
41 loam soil. The colour map indicates water distribution within the soil column.

42

43 **Key Words:** Wheat, Root architecture, Neutron Computed tomography; Water dynamics

44 **1. Introduction**

45 The seemingly insurmountable task of feeding a growing global population with increasingly
46 limited natural resources is one of the greatest challenges facing humanity in the 21st century
47 (Borlaug and Dowsell, 2003; Lal, 2016). With the effects of climate change threatening to
48 further disturb global production patterns across the world, it is imperative for the research
49 community to devise possible strategies to increase global crop productivity in the
50 forthcoming decades (IPCC, 2007; Knox et al., 2012). This will require a deeper
51 understanding of factors affecting crop production systems using contemporary technologies.

52 One such area of research that has received increased attention of late is that of below ground
53 root-soil interactions. These interactions are a vital part of the crop production system as
54 plants acquire the majority of the resources they use for production via these associations and
55 thus increasing our understanding of these interactions may hold the key for a ‘second green
56 revolution’ required to feed a rapidly growing population (Gewin, 2010; Lynch, 2007; Rich
57 and Watt, 2013).

58 Understanding root-soil interactions especially amongst the worlds’ major cereal crops
59 (maize, wheat, rice) is of paramount importance for the attainment of sustainable global food
60 security as these crops provide more than two thirds of all human dietary energy (Cassman,
61 1999; FAOSTAT, 2019; Khoury et al., 2014). This understanding is crucial for wheat in
62 particular as it is arguably the worlds’ most important staple food crop. It accounts for more
63 than 15% (220 million ha) of global arable land use, (the highest for any cultivated plant)
64 and often yields in excess of 700 million metric tonnes of grain per annum globally
65 (FAOSTAT, 2019). In spite of its great importance however, yield gaps in wheat production
66 still exist, often as a result of poor adaptation of its root system to varying edaphic conditions
67 (Senapati and Semenov, 2019; Waines and Ehdaie, 2007). As such increased research into
68 root-soil interactions in wheat to tailor its root system for different soil environments is

69 pivotal for improving wheat yields especially in marginal areas (Alahmad et al., 2019;
70 Figueroa-Bustos et al., 2018; Waines and Ehdaie, 2007).

71 Traditionally these root-soil interactions have been investigated using either inference root
72 health from the development of above ground parts (shoots) or by the more labour intensive
73 invasive soil excavation methods (Pierret, et al. 2005). These observations however, although
74 useful, lacked critical root developmental detail required to make conclusive inferences into
75 how best to improve plant productivity (Mooney et al., 2012). Even when elements of the
76 root-soil interactions were deduced, high throughput measurements were often very difficult
77 to obtain which limited research into subterranean interactions.

78 The advent of non-invasive soil imaging in the late 70's marked a significant step forward in
79 the study of plant-soil interactions with technologies such as X-Ray Computed Tomography
80 (X-Ray CT) (Crestana, et al, 1986; Keyes et al., 2013; Tracy et al., 2013; Ahmed et al., 2016;
81 Blunk et al., 2017; Burr-Hersey et al., 2017; Koebernick et al., 2017), Magnetic Resonance
82 Imagery (MRI) (Metzner et al., 2015; Pflugfelder et al., 2017; Stingaciu et al., 2013), Nuclear
83 Magnetic Resonance imaging (NMR)(Bačić and Ratković, 1987; Brown et al., 1991;
84 Southon, et al, 1992) and Neutron imaging (NI) (Willatt, et al, 1978; Furukawa, et al. 1999;
85 Menon et al., 2007; Tötze et al., 2017) being used to answer a multitude of questions about
86 root-soil interactions in great detail. Of these technologies NI has been the most effective
87 non-invasive soil imaging technique used when studying water dynamics and root growth
88 within the soil due to its high sensitivity to hydrogen which is abundant in water (Robinson,
89 et al. 2008). Willatt. et al, (1978), demonstrated the use of this method for the first time,
90 successfully imaging roots of different plants (soya bean and maize) growing in soil.
91 Subsequently this technology was used by in many studies including Willatt and Struss
92 (1979), Couchat et al., (1980), Bois and Couchat, (1983), (Nakanishi, et al 1992) as well as
93 Furukawa, et al. (1999). Two papers by Menon et al (2007) and Moradi et al., (2009) also

94 provided a comprehensive, accurate description of NI that subsequently led to even more
95 insightful studies using NI.

96 Initial plant experiments with NI involved the use of 2 dimensional neutron radiography (NR)
97 to study the root architectural properties in situ (Bois and Couchat, 1983; Couchat et al.,
98 1980; Willatt and Struss, 1979) using thin slabs made of aluminium. The most extensively
99 used plants in NI have been maize (*Zea mays* L.) pioneered in experiments by Willatt, et al.
100 (1978) and lupine (*Lupinus albus* L.) first used by Nakanishi, et al. (1992) with the majority
101 of papers being published on NI in plant-soil interaction mainly focusing on them. Research
102 in soil NI has since moved on to the study of more complex root-soil processes such as
103 dynamics of water flux and the extent of rhizosphere which had previously been difficult to
104 study using other techniques (Carminati et al., 2010; Oswald et al., 2008). Visualisation of
105 water movement coupled with the ability to use tracers such as heavy water (D_2O) in NI has
106 led to a better understanding of water uptake and transport in specific roots with
107 Zarebanadkouki, et al. (2013) showing that most of the water uptake in 3 week old lupine
108 plants is carried out by the lateral roots with the tap root mainly acting as a conduit for
109 upwards water movement.

110 Unlike NR, there have been fewer studies that have used neutron computed tomography
111 (NCT) to study soil-root water dynamics despite the fact that computed tomography has the
112 potential to provide even more detailed 3D visualisation of plant-soil systems as compared to
113 NR. Its uptake may have been limited by the size of the specimen that can be successfully
114 imaged in detail (usually no more than 20mm in diameter) as well as the time required for
115 such images to be taken, which is much longer than that for individual neutron radiographs
116 (Warren et al., 2013). The initial work done by Tumlinson et al., (2008) and Esser et al.,
117 (2010) with maize seedlings and lupine seedlings showed that visualisation of root and water
118 distribution dynamics in soils can be visualised successfully in 3D using NCT with improved

119 root-soil contrast as compared to other non-invasive imaging techniques. Moradi et al.,
120 (2011) went a step further in their study with lupine plants showing that water dynamics at
121 the microscale can be accurately observed in 3D and thus can be used in complex and precise
122 modelling operations explaining rhizosphere water flux. Recent advancement in NCT by
123 Zarebanadkouki et al., (2015) who visualised 3D water dynamics of lupine plants in real
124 time, provide great prospects of the use of NCT in further plant-soil interaction studies.

125 Regardless of the recent advancements in NCT in plant-soil interaction studies, there are
126 some important limitations for this technique. For example, all of the previous studies
127 utilising NCT have used soils containing no less than 90% sand, which are mostly devoid of
128 organic matter or macro-aggregates. Therefore, for a wider application of this method it will
129 require testing further using a variety of soil textures and structures. Also conspicuous in
130 many NI studies to date is the absence wheat root architectural investigations using this
131 technology despite the crop being major contributor to global food security. As such it is
132 important to test the feasibility of the use of NI on wheat plants, with the aim of enhancing
133 knowledge on wheat roots and their interactions with soil moisture.

134 In this paper, we thus aimed at determining the 3D root architecture of wheat seedlings grown
135 in an aggregated sandy loam soil with 4% organic matter content using NCT. Our specific
136 objectives were to use NCT to: a) Map 3D wheat root architectural distribution within an
137 aggregated sandy loam soil b) Visualise in 3D, soil water distribution after a brief drying
138 period and (c) to understand how the root system architecture interacts with soil moisture
139 distribution as brought about by soil structural heterogeneity within an aggregated soil.

140

141

142

143 2. Materials and methods

144 2.1 Sample preparation and plant growth

145 The soil used in this experiment was a sandy loam soil (70% Sand, 17% Clay, and 13% Silt)
146 obtained from Cove farm (53°30'03.7"N 0°53'57.2"W) and had an organic carbon content of
147 5.59%. This soil was air dried and mechanically sieved through a 4mm sieve to eliminate
148 large clods and aggregates. The sieving produced a dry aggregate size distribution of 24% for
149 particles <250 μ m, 36% for 250-500 μ m, 13% for 500-1000 μ m, 13% for 1000-2000 μ m and
150 14% for 2000-4000 μ m with 4% SOM. This was then packed into specially designed, closed
151 bottom, cylindrical aluminium tubes (18mm internal diameter \times 100mm height) to ensure a
152 bulk density of 1.2g cm⁻³ within the tubes. A single wheat (*Triticum Aestivum*. L cv. Fielder)
153 seed was sown about 1cm underneath the surface of the soil and the tubes were watered to a
154 volumetric moisture content (θ) of 16.0 \pm 3.0% which was experimentally determined (using
155 gravimetric methods) to be the field capacity of our growth tubes. This water content was
156 maintained during the course of this experiment by daily surface irrigation to the
157 predetermined weight corresponding to the above mentioned θ for each tube. The wheat
158 seedlings were grown for 13 days (starting from date of planting) in a growth chamber
159 maintained at a temperature of 22°C (day)/18°C (night) and a relative humidity of 55% with
160 light intensity averaging 400 μ mol m² s⁻¹ with an 8-hour day length. Watering was stopped 4
161 days before neutron imaging was carried out to enhance the contrast between the root and
162 soil.

163 2.2 Neutron computed tomography set up

164 Neutron CT imaging was carried out at the IMAT neutron imaging beamline of the ISIS
165 Neutron and Muon Source at the Rutherford Appleton Laboratory, UK. A more detailed
166 description of the IMAT imaging station can be found in (Burca et al., 2013); Kockelmann et

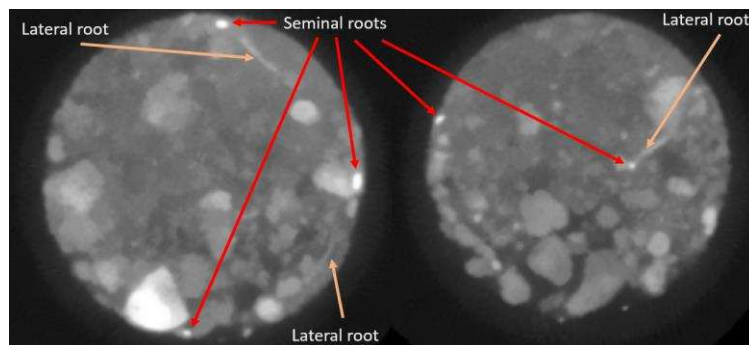
167 al., 2013 and Burca et al., 2018). For these experiments the neutron beam was shaped to the
168 field of view of 112.7 mm × 112.7 mm accompanied by a multiaxial tomography stage
169 allowing for 2 simultaneous scans. The neutron radiographies were acquired with an optical
170 camera box equipped with Andor Zyla 4.2 PLUS sCMOS with 2048×2048 pixels, an 85mm
171 lens and 100 μm 6LiF/ZnS: Ag scintillator. The images produced had a pixel and voxel size
172 of 55μm with 30s being the exposure time for each projection and an L(10000mm) /D
173 (40mm)= 250. The time taken for a single scan of the plants was almost 6 hours with 654
174 radiographs being recorded using a rotation step of 0.55°. This was the best set up achievable
175 on IMAT, suitable for our experiment (Mawodza et al., 2018).

176 2.3 Image reconstruction, root segmentation and analysis

177 The images were reconstructed using the commercial available Octopus 8.9 software
178 (Octopus, 2019), and images were corrected for neutron beam variation and camera noise
179 using the flat images and dark images taken before and after image acquisition (Dierick et al.,
180 2004; Vlassenbroeck et al., 2006). We did not use an scattering correction when processing
181 our images. The final reconstructed stack of images were imported into Avizo ® 9.0.1 for
182 root segmentation and analysis (FEI, 2015).

183 We attempted to use automated root segmentation algorithms RooTrack (Mairhofer et al.,
184 2012) and Root1 (Flavel et al., 2017) but due to the great heterogeneity in water content both
185 the soil and within roots, these proved unreliable for our samples. To get the best results,
186 roots were manually segmented using the limited range paintbrush editor in the segmentation
187 module in Avizo software. The segmented roots obtained from this process were then used to
188 calculate root lengths, thickness, surface area and volume for each root scan. Segmentation of
189 the larger seminal roots was primarily done using automated thresholding techniques
190 available in Avizo as there was a clear attenuation contrast between the soil and these roots.

191 This was however not done universally throughout the whole root system as most of the
192 smaller lateral roots as well as some sections of the larger seminal roots had attenuation
193 values that poorly contrasted or were even lower than that of moist soil and aggregates
194 surrounding them as shown in Figure 2. Time consuming manual segmentation based on a
195 combination of localised differences in attenuation and the connectivity of circularly shaped
196 pixel groups (as roots are usually circular in shape) enabled the segmentation of the
197 outstanding lateral roots and seminal root sections throughout the soil columns. Calibration
198 for water content was done using the same soil used in our experiments with known
199 volumetric water contents similar to what was done in Moradi et al., (2011). We then used
200 this calibration to relate the relative neutron attenuation to the moisture content for all the
201 images we acquired.



202
203 Figure 2: Grayscale images used to segment out roots showing how the different root types
204 contrasted with the soil.
205

206 2.4 WinRhizo® root analysis

207 As segmentation was a subjective process, we compared the root properties obtained from
208 our analysis with those obtained from flatbed scanning results analysed using WinRhizo ®
209 (Regents Instruments, Inc.). Therefore, after CT scanning, the soils columns were
210 destructively sampled and the soil was washed off from the roots over a 250µm sieve. The
211 washed roots were then placed in a specially designed water tray and scanned using an Epson

212 Expression 10000XL Pro at 600dpi resolution. This scan obtained 2D images of the plant
213 roots which were then analysed using WinRHIZO® 2016a software to determine the root
214 properties (Wang and Zhang, 2009). These roots alongside their shoots were then dried at
215 65°C for 48 hours to obtain their dry biomass.

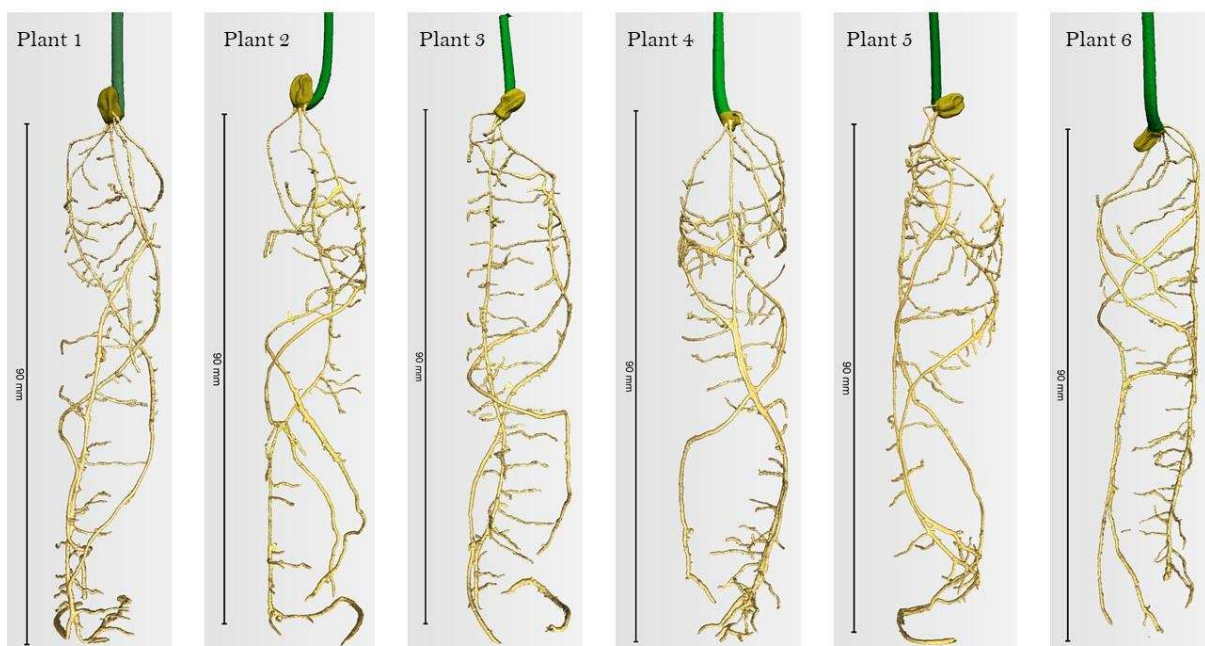
216 2.5 Statistical analysis

217 All graphs and statistical analysis for these experiments was performed using GraphPad
218 Prism 8.0.1 (<https://www.graphpad.com/>) with a two tailed paired T tests used to separate
219 means.

220 3. Results

221 3.1 3D wheat root architecture from NCT

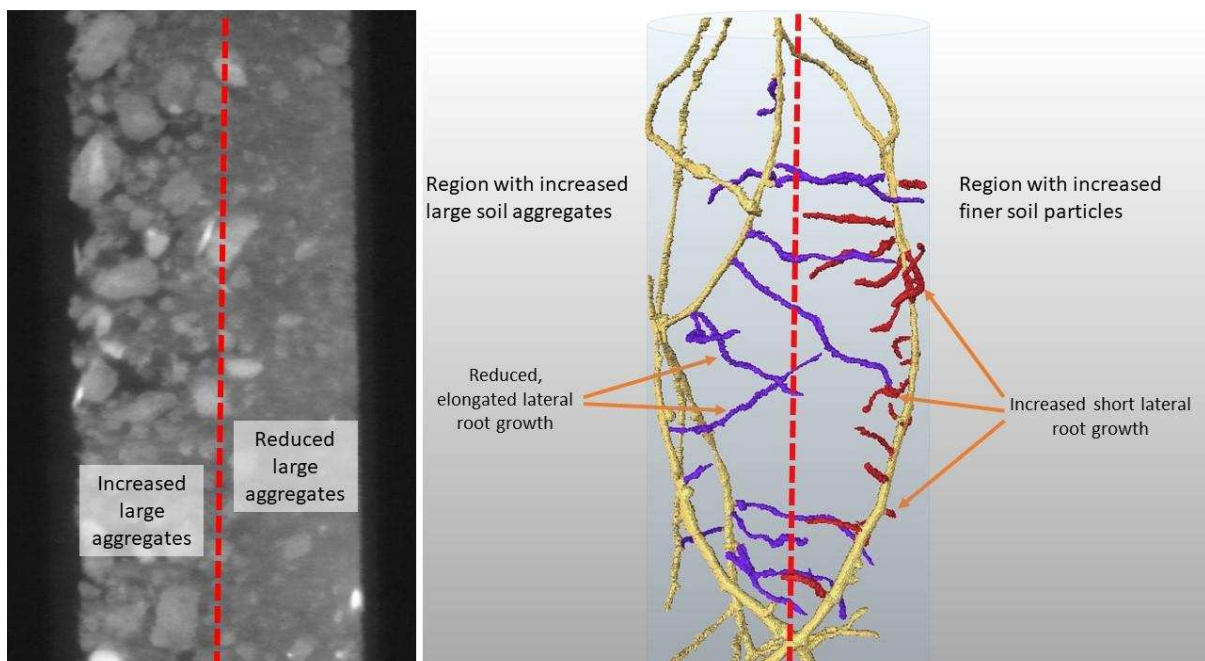
222 Three-dimensional root architectural properties of the 13-day old wheat seedlings rendered
223 from neutron scanning were successfully mapped with images in Fig 3. illustrating the
224 different root systems of the six plants that were grown.



225

226 Figure 3: Images revealing the root architecture of the 6 different plants grown

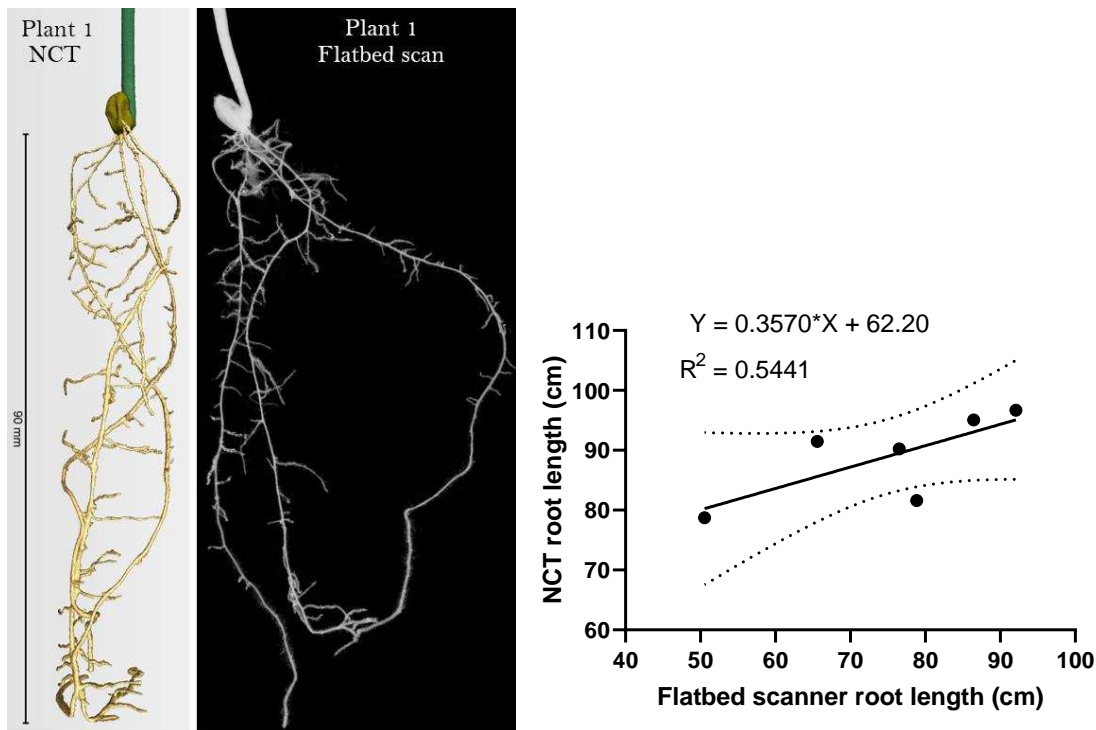
227 The root architecture of the plants was broadly similar with an average total root length of
 228 89.775 cm \pm 4.418 (SEM). The plants had 3-5 seminal roots at the time of imaging with least
 229 one of the roots (mainly the primary root) having grown to reach to the base of the growth
 230 tube they were growing in. Lateral roots of the different plants extended throughout the soil
 231 column with visible differences in lateral root growth especially in regions where the seminal
 232 roots were in close proximity to larger aggregates (1-4mm) that had large pores in-between
 233 them. Lateral roots growing in these regions tended to be fewer and longer whilst those
 234 growing in finer soil particles were more numerous but visibly shorter. This can be seen in
 235 Figure 4 where due to the random segregation of particles when packing, larger aggregates
 236 settled on one side of the column. Roots in some of the columns (plant 1, 4 and 6 in Figure 3)
 237 also coalesced together and grew side by side in their downwards trajectory, only
 238 disentangling lower down the soil column.



239
 240 Figure 4 (Left)Greyscale image of a growth tube showing a segregation of large aggregates
 241 towards the left side of growth tube. (Right) increased shorter lateral root growth in regions
 242 with finer soil particles whilst lateral roots growing in regions with increased larger
 243 aggregates are reduced and longer. The red line demarcates an arbitrary boundary between
 244 regions dominated by large aggregates or finer particles. Longer lateral roots are shown in
 245 purple whilst short lateral roots are shown in red.

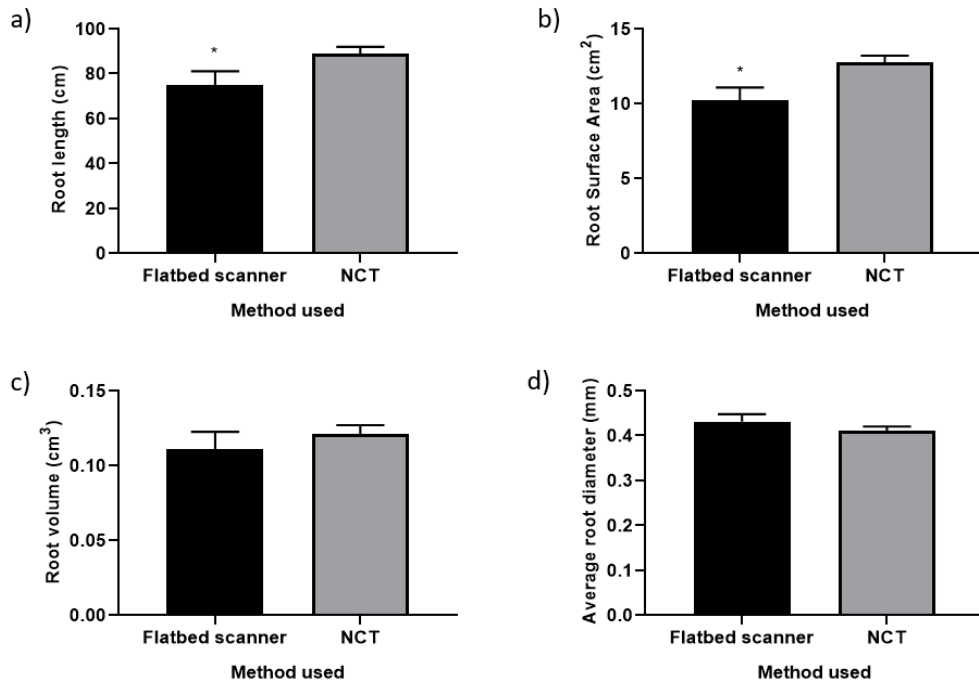
246 3.2 Comparison between 3D and 2D root properties

247 Root properties calculated using WinRhizo® from the flatbed scanning and 3D NCT enabled
248 the correlation of the two methods thus ensuring the validity of the method we used to
249 segment out the roots. Visual comparison between images obtained using the two methods as
250 shown in Figure 5 showed great similarities between them.



251
252 Figure 5: Side by side comparison of the same plant imaged using NCT and flatbed scanning
253

254 There was also a moderately strong linear relationship ($R^2= 0.5441$) between the root length
255 estimated by the two methods as given in Figure 5. As shown in Figure 6, estimates of root
256 length and surface area from neutron scans were significantly ($P<0.05$) higher than those
257 from flatbed scanning whilst root volume and thickness did not vary between the two
258 methods. The thinnest roots we could detect were around $110\mu\text{m}$ (2 voxels) in diameter
259 which corresponds to double our image pixel size according to Nyquist–Shannon theorem.

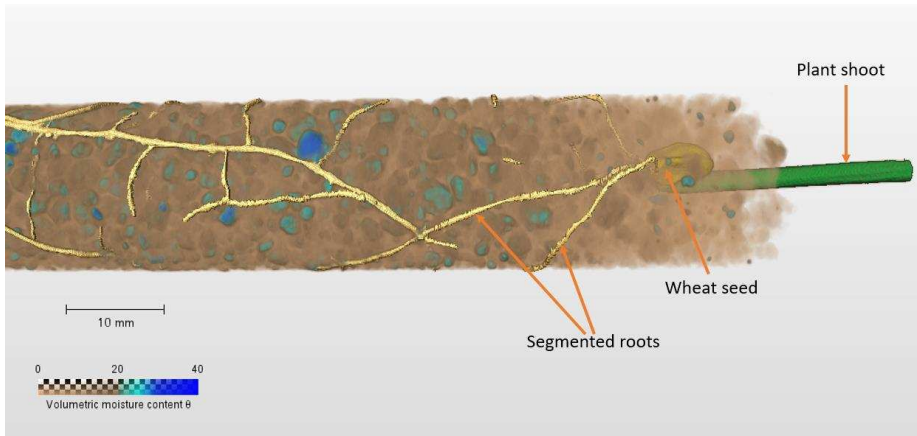


260

261 Figure 6: Comparison of root architectural properties as estimated by flatbed scanning and
 262 NCT. a) Root length ($P= 0.0250$), b) Root surface area, c) Root volume and d) Average root
 263 diameter. The error bars indicate Standard Error of the mean and * indicates significant
 264 differences ($P < 0.05$)
 265

266 3.3 Soil moisture distribution

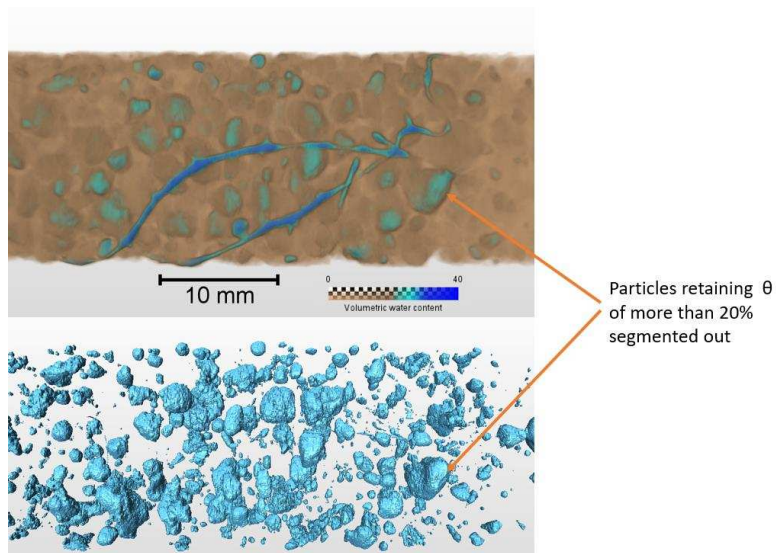
267 Similar to root architecture, the visualisation of soil moisture distribution was possible in 3D
 268 NCT as illustrated in Figure 7 with neutron attenuation being used as a proxy for θ using
 269 calibrated estimates of water content. These were calibrated by a series of scans of dry soil
 270 samples similar (but not identical) to those used for plant growth. It is worth noting however
 271 that our estimation of moisture content may encompass an add on effect with the high organic
 272 matter which increases neutron attenuation.



273

274 Figure 7: 3D NCT rendering of water distribution in aggregated soil where wheat seedling is
 275 growing
 276

277 Water distribution within the columns was sporadic with regions of increased moisture
 278 localisation and depletion throughout the different tubes. Water depletion was greatest in the
 279 top 20mm of the soil with soil moisture gradually increasing between 20-60mm from the top
 280 of the column until it reached its greatest extent at the base of the tube. Water was largely
 281 localised in regions with nearly spherically shape regions within the soil as shown in Figure
 282 8. Upon further analysis, it was discovered that this moisture accumulation was mainly
 283 associated with the heterogeneously distributed soil aggregates within the soil. As compared
 284 to finer particles, all or parts of aggregates have a $\theta > 20\%$.

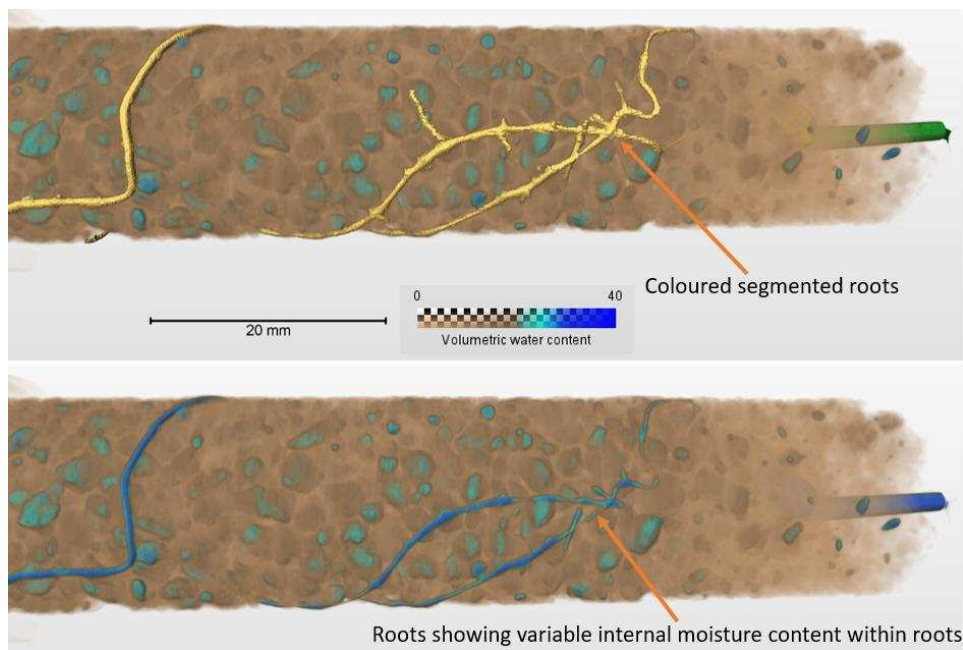


285

286 Figure 8: Showing segmenting out of particles retaining greater $\theta > 20\%$

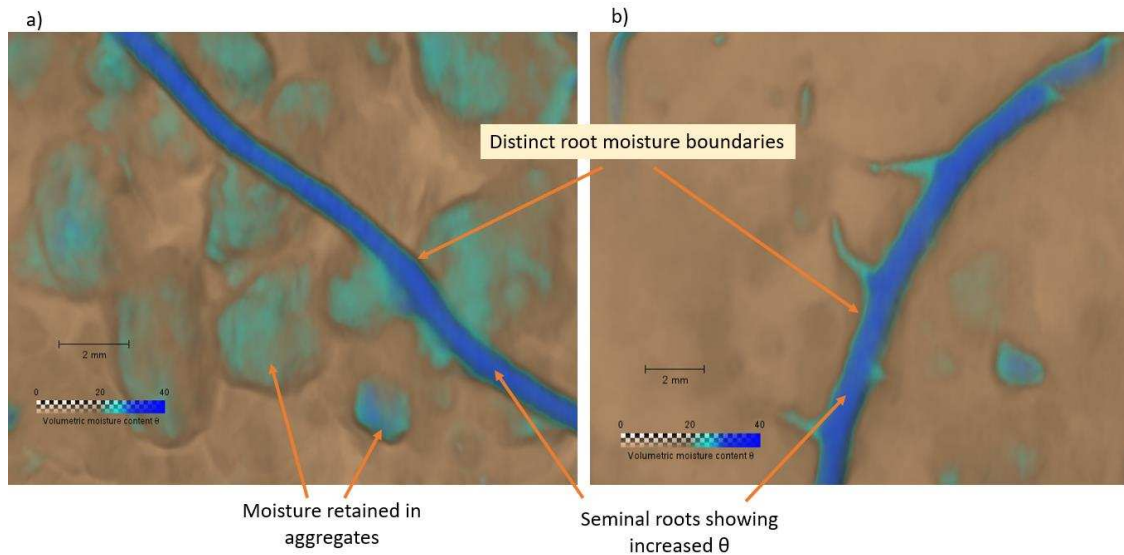
287 3.4 Root interactions with soil moisture

288 Wheat roots did not preferentially grow in regions of increased θ (blue regions with $\theta > 20$).
289 Many of the roots that were observed did not penetrate into water rich aggregates but rather
290 grew around them. Roots that were in direct contact with aggregates with a higher θ exhibited
291 an increase in their internal θ . In large pores in-between soil aggregates, roots had reduced θ
292 which was especially true in smaller lateral roots as opposed to the much larger seminal root
293 network. Some seminal roots however also showed this unexpected internal θ decrease when
294 growing through larger inter-aggregate pores. The rhizosphere around the roots as shown in
295 Figure 10, did not show great differences in θ as compared to the rest of the soil with
296 delineation of the extent of the rhizosphere being difficult decipher.



297

298 Figure 9: Variations in internal water content within roots growing through soil. The top
299 image shows segmented root indicated in yellow whilst in the bottom image, only root
300 moisture content can be visualised
301



302

303 Figure 10: Close up view of the water-map in around seminal roots at a) 3cm and b) 5 cm
 304 below the soil surface showing distinct boundaries around the roots

305 **4. Discussion**

306 4.1 3D NCT wheat root architecture

307 The results presented show that detailed 3D root architectural properties of wheat growing in
 308 an aggregated soil with a moderately high organic matter content can successfully be
 309 visualised using NCT. To the best of our knowledge, this is the first study to use NCT to
 310 study root architectural development in wheat plants in detail. This research also represents a
 311 significant step away from many of the previous NCT root architectural studies such as those
 312 done by Nakanishi et al., (2005), Moradi et al., (2011), Warren et al., (2013) and Tötze et
 313 al., (2017) that have used predominantly sand soils (with >90% sand). The sand soils used in
 314 the previously mentioned studies are more or less homogeneous and often lack aggregation.
 315 This study thereby seeks to break with convention by using a heterogeneous, aggregated soil
 316 with increased SOM. We recognise however, that the use of an aggregated soils as in this
 317 study presents a potential challenge when attempting to segment out wheat roots. This
 318 difficulty is brought about by the heterogeneity in soil properties with isolated regions
 319 retaining increased moisture and/or being high in organic matter (e.g. soil aggregates) that are

320 highly neutron attenuating due to their increased hydrogen content (Robinson, et al. 2008).
321 As a consequence of such features, there is a reduction in the clear attenuation difference
322 between the soil and plant root matter that is characteristic in sand soils thus complicating
323 segmentation as simple thresholding would yield inaccurate results. In this study we were
324 able to overcome such difficulty by both localised thresholding using the increased
325 attenuation and interconnectivity between roots as well as intuitive manual segmentation
326 techniques.

327 This study represents a move away from the use of the leguminous dicotyledonous plant
328 lupine (*Lupinus albus*. L) that has been popularly studied in many NCT and neutron
329 radiography experiments ever since the pioneering work of (Nakanishi, et al. 1992) and then
330 Menon et al., (2007) who established this plant as a ‘model’ for non-invasive neutron
331 imaging studies in plant-soil systems (Zarebanadkouki et al., 2012; Rudolph-Mohr, et al.
332 2014; Ahmed et al., 2017). Our use of the monocotyledonous gramineae family plant, wheat
333 represents one of the first attempts at visualising the RSA of a staple food crop using NCT.
334 Many of the non-invasive imagery done on wheat plants has been carried out exclusively
335 using X-Ray CT (Flavel et al., 2014, 2012; Jenneson et al., 1999; Mooney et al., 2006; Tracy
336 et al., 2012). This study thereby demonstrates the feasibility of using NCT to study the RSA
337 of not only wheat plants but also other staple monocotyledonous crops such as rice and
338 maize.

339 4.2 Comparison between 3D and 2D root properties

340 As the manual segmentation methods we used to reveal root architecture from NCT scans
341 could be subjective, a comparison between the results obtained from NCT scanning and
342 flatbed scanner scanning was done. This is the first time results from NCT have been
343 compared to images flatbed scanning results. Similar correlations have previously been done

344 in on X-Ray CT scan root measurements such as those by Tracy et al., (2015) and Flavel et
345 al., (2012). In this study, here was moderately good correlation ($R^2 = 0.54$) between the two
346 methods with respect to key essential root characteristics, root length and volume with
347 estimates from flatbed scanning being significantly lower in root length. This could be
348 explained by the fact that some roots are inevitably lost during washing with literature
349 estimating a loss of about 20-40% of dry matter during storage and washing operations for
350 wheat roots (van Noordwijk and Floris, 1979; Grzebisz. et al, 1989). These losses though,
351 may be partially compensated for by the inability of our NCT to measure and quantify roots
352 less than 110 μm ($55\mu\text{m}$ pixel size $\times 2$) which is 2 times each voxel size that is widely
353 regarded as the effective spatial resolution limit of CT images (Moradi et al., 2011). Roots of
354 this thickness can be picked up by flatbed scanning provided they are not lost during the
355 washing process.

356 4.3 Soil moisture distribution

357 Similar to root system architecture, visualisation of soil moisture distribution was possible in
358 3D with the greyscale intensity acting as a proxy for θ . The high soil moisture heterogeneity
359 within the scanned tubes was as expected since soil heterogeneity often results in variable
360 hydraulic conductivity throughout the soil which has a direct bearing on the θ in unsaturated
361 conditions. As plants were surface irrigated, θ was lowest at the soil surface increasing
362 steadily towards the base of the growth tube. This accumulation of water at the base of the
363 tubes may have been brought about by the lack drainage as they were sealed at the base to
364 allow for accurate determination of the gravimetric water content. Localisation of water as
365 shown in Figure 8, which was presumed to be as a result to the preferential retention of water
366 in aggregates. This preferential water retention was presumed to arise from the pore size
367 distribution within soil aggregates which is often comprised of multiple micro-pores with the
368 ability to store water at higher suctions as opposed to the inter-aggregate pores referred to in

369 literature as structural pore spaces that are characteristically bigger and thus can freely
370 transmit water. This preferential water retention however was not universal as some
371 aggregates were also relatively dry at the time of imaging with some parts of the moist
372 aggregates also being relatively drier as compared to the rest of the aggregate. This may
373 suggest that that some aggregates may have pores large enough to drain freely at lower
374 suction levels.

375 Inference of soil moisture status using NCT and neutron radiography is not new with several
376 scholars having shown soil moisture distribution in sand soils. This study builds on their
377 findings adding further complexity by looking at an aggregated soil that has an increased
378 organic matter content. This introduces inaccuracies with the estimation of water content as
379 in such a soil, water is not the only highly neutron attenuating substance as organic matter has
380 increased hydrogen atom content as compared to soil (Robinson, et al. 2008; Tumlinson et
381 al., 2008). This thus means the total attenuation of each voxel is dependent on the water
382 content as well as the organic matter content for the particular volume of soil under review.
383 In this study we calibrated for water content using the same soil at varying levels of θ ,
384 however in doing this we assumed that the organic matter content throughout the soil was
385 constant and variation in attenuation was primarily due to increased soil moisture content.
386 This estimation would be inaccurate especially in regions with localised elevated level of soil
387 organic matter. As such our interpretation of soil moisture distribution should be taken with
388 this in consideration.

389 4.4 Root interactions with soil moisture

390 As roots did not seem to grow preferentially in regions of relative high θ (are not highly
391 hydrotropic), it is clear that many other factors such as gravity, pore size distribution and
392 nutrient status of the soil may have also contributed to root growth patterns (Kar, et al. 1979;

393 Niu et al., 2015; Sato et al., 2015). As roots grew around different aggregates probably as a
394 consequence of trying to find the path of least resistance, many of the roots had good contact
395 with the surface of the moist aggregates. Roots in contact with moist aggregate surfaces
396 seemed to be able to extract water from these aggregates as more often than not, these roots
397 exhibited an increased in θ . It was striking however that roots growing through large air
398 spaces within the soil in some cases seemed to exhibit a reduction in θ as they passed through
399 the pore space. This is thought to be as a result of increased evaporative water loss from the
400 root surface within these large air spaces. Such large inter-aggregate pores may thus act as a
401 hindrance to internal root hydraulic conductivity and thus limiting the functionality of roots
402 growing through them. This finding could in part explain some of the observations seen by
403 (Passioura and Stirzaker, 1993) as well as Alexander and Miller (1991) who noticed a
404 general reduction in plant growth when artificial holes are introduced or when plants are
405 grown soils with large aggregate sizes.

406 Another unexpected result from our study was the absence of a distinct region of increased θ
407 around the roots demarcating rhizosphere soil around the roots as shown in Figure 10. This is
408 contrary to what has been observed in many neutron studies such as those done by (Moradi et
409 al., 2011) who noticed this distinct feature in all the plants they studied. This variation could
410 be as a result of our use of a different textured soil that may not produce such distinct features
411 as soil moisture was heterogeneously distributed within the soil. Differences in plant species
412 difference i.e. wheat used in this study as compared to maize or lupins mainly used in
413 previous studies could also be a contributory factor to our observed differences. Another
414 plausible explanation for this could be in the difference of root segmentation protocols that
415 were used in the different studies. In this case where semi-automatic and manual
416 segmentation was employed based on the roots distinct increased attenuation properties, the
417 edges of the roots could be mistaken to lie within the rhizosphere. This is however unlikely as

418 the root thickness as estimated NCT compare well to that found by flatbed scanning.
419 Questions may also be asked about the demarcation of root boundaries in the previous studies
420 as many of these studies did not compare the thickness of the roots found in their scans to
421 those obtained by manual measurement.

422 **5. Conclusion**

423 NCT was found to be able to reveal root architecture of wheat plants grown in an aggregated
424 sandy loam soil with appreciable amounts of organic matter and inherent heterogeneity. This
425 marks a step forward from the use of predominantly sand soils in NCT, albeit with new
426 challenges of its own. Macro-aggregates increased water storage within the soil with their
427 heterogeneous distribution determining the water distribution patterns across the soil after a
428 period of drying which could help plants water acquisition in times of limited water supply.
429 Lateral root growth was found to be reduced in regions with increased macro aggregates with
430 roots growing through large inter-aggregate pores exhibiting loss of moisture that could
431 potentially limit root function. Our work highlights how soil heterogeneity may affect water
432 distribution and plant-soil interactions thus encouraging the further use of NCT technology to
433 answer questions related soil water distribution in heterogeneous media for better modelling
434 of soil water movement.

435 **Funding and Acknowledgements**

436 This research was funded as part of a PhD studentship by the Grantham Centre for
437 Sustainable Futures at the University of Sheffield. Neutron imaging beamline grant
438 (RB1820361) was provided by STFC ISIS Facility from Rutherford Appleton Laboratory,
439 UK (Mawodza et al., 2018).

440 **Conflicts of Interest**

441 The authors declare no conflict of interest. The funders had no role in the design of the study;
442 in the collection, analyses, or interpretation of data; in the writing of the manuscript, or in the
443 decision to publish the results.

444 **References**

- 445 Ahmed, M.A., Zarebanadkouki, M., Ahmadi, K., Kroener, E., Kostka, S., Kaestner, A.,
446 Carminati, A., 2017. Engineering Rhizosphere Hydraulics: Pathways to Improve Plant
447 Adaptation to Drought. *Vadose Zo. J.* 0, 0. <https://doi.org/10.2136/vzj2016.09.0090>
- 448 Ahmed, S., Klassen, T.N., Keyes, S., Daly, M., Jones, D.L., Mavrogordato, M., Sinclair, I.,
449 Roose, T., 2016. Imaging the interaction of roots and phosphate fertiliser granules using
450 4D X-ray tomography. *Plant Soil* 401, 125–134. [https://doi.org/10.1007/s11104-015-](https://doi.org/10.1007/s11104-015-2425-5)
451 [2425-5](https://doi.org/10.1007/s11104-015-2425-5)
- 452 Alahmad, S., El Hassouni, K., Bassi, F.M., Dinglasan, E., Youssef, C., Quarry, G., Aksoy,
453 A., Mazzucotelli, E., Juhász, A., Able, J.A., Christopher, J., Voss-Fels, K.P., Hickey,
454 L.T., 2019. A Major Root Architecture QTL Responding to Water Limitation in Durum
455 Wheat. *Front. Plant Sci.* 10, 436. <https://doi.org/10.3389/fpls.2019.00436>
- 456 Bačić, G., Ratković, S., 1987. NMR studies of radial exchange and distribution of water in
457 maize roots: The relevance of modelling of exchange kinetics. *J. Exp. Bot.* 38, 1284–
458 1297. <https://doi.org/10.1093/jxb/38.8.1284>
- 459 Blunk, S., Malik, A.H., de Heer, M.I., Ekblad, T., Bussell, J., Sparkes, D., Fredlund, K.,
460 Sturrock, C.J., Mooney, S.J., 2017. Quantification of seed-soil contact of sugar beet
461 (*Beta vulgaris*) using X-ray Computed Tomography. *Plant Methods* 13, 1–14.
462 <https://doi.org/10.1186/s13007-017-0220-4>
- 463 Bois, J.F., Couchat, P.H., 1983. Comparison of the Effects of Water Stress on the Root

464 Systems of Two Cultivars of Upland Rice (*Oryza sativa* L.). *Ann. Bot.* 52, 479–487.

465 Borlaug, N., Dowswell, C., 2003. Feeding a world of ten billion people: a 21st century
466 challenge. ... *Int. Congr. Wake* ... 3–23.

467 Brown, D.P., Pratum, T.K., Bledsoe, C., Ford, E.D., Cothorn, J.S., Perry, D., 1991.
468 Noninvasive studies of conifer roots: nuclear magnetic resonance (NMR) imaging of
469 Douglas-fir seedlings. *Can. J. For. Res.* 21, 1559–1566.

470 Burca, G., Kockelmann, W., James, J.A., Fitzpatrick, M.E., 2013. Modelling of an imaging
471 beamline at the ISIS pulsed neutron source. *J. Instrum.* 8. [https://doi.org/10.1088/1748-](https://doi.org/10.1088/1748-0221/8/10/P10001)
472 [0221/8/10/P10001](https://doi.org/10.1088/1748-0221/8/10/P10001)

473 Burca, G., Nagella, S., Clark, T., Tasev, D., Rahman, I.A., Garwood, R.J., Spencer, A.R.T.,
474 Turner, M.J., Kelleher, J.F., 2018. Exploring the potential of neutron imaging for life
475 sciences on IMAT. *J. Microsc.* 00, 1–6. <https://doi.org/10.1111/jmi.12761>

476 Burr-Hersey, J.E., Mooney, S.J., Bengough, A.G., Mairhofer, S., Ritz, K., 2017.
477 Developmental morphology of cover crop species exhibit contrasting behaviour to
478 changes in soil bulk density, revealed by X-ray computed tomography. *PLoS One* 12, 1–
479 18. <https://doi.org/10.1371/journal.pone.0181872>

480 Carminati, A., Moradi, A.B., Vetterlein, D., Vontobel, P., Lehmann, E., Weller, U., Vogel,
481 H.J., Oswald, S.E., 2010. Dynamics of soil water content in the rhizosphere. *Plant Soil.*
482 <https://doi.org/10.1007/s11104-010-0283-8>

483 Cassman, K.G., 1999. Ecological intensification of cereal production systems: yield potential,
484 soil quality, and precision agriculture. *Proc. Natl. Acad. Sci. U. S. A.* 96, 5952–9.
485 <https://doi.org/10.1073/pnas.96.11.5952>

486 Couchat, P., Moutonnet, P., Houelle, M., Picard, D., 1980. In situ study of corn seedling root

487 and shoot growth by neutron radiography. *Agron. J.* 72, 321-324 ST-In situ study of
488 corn seedling root.

489 Crestana, S., Cesareo, R., Mascarenhas, S., 1986. Using a computed tomography miniscanner
490 in soil science. *Soil Sci.* 142, 56–61.

491 Dierick, M., Masschaele, B., Van Hoorebeke, L., 2004. Octopus, a fast and user-friendly
492 tomographic reconstruction package developed in LabView. *Meas. Sci. Technol.* 15,
493 1366–1370. <https://doi.org/10.1088/0957-0233/15/7/020>

494 Esser, H.G., Carminati, A., Vontobel, P., Lehmann, E.H., Oswald, S.E., 2010. Neutron
495 radiography and tomography of water distribution in the root zone. *J. Plant Nutr. Soil*
496 *Sci.* 173, 757–764. <https://doi.org/10.1002/jpln.200900188>

497 FAOSTAT, 2019. FAOSTAT database [WWW Document]. Food Agric. Organ. United
498 Nations, Rome, Italy. URL <http://www.fao.org/faostat/en/#home>

499 FEI, 2015. User's guide Avizo ® 9 [WWW Document].

500 Figueroa-Bustos, V., Palta, J., Chen, Y., Siddique, K., 2018. Characterization of Root and
501 Shoot Traits in Wheat Cultivars with Putative Differences in Root System Size.
502 *Agronomy*. <https://doi.org/10.3390/agronomy8070109>

503 Flavel, R.J., Guppy, C.N., Rabbi, S.M.R., Young, I.M., 2017. An image processing and
504 analysis tool for identifying and analysing complex plant root systems in 3D soil using
505 non-destructive analysis : Root1 1–18. <https://doi.org/10.7910/DVN/DXG4AH.Funding>

506 Flavel, R.J., Guppy, C.N., Tighe, M., Watt, M., McNeill, A., Young, I.M., 2012. Non-
507 destructive quantification of cereal roots in soil using high-resolution X-ray tomography.
508 *J. Exp. Bot.* 63, 2503–2511. <https://doi.org/10.1093/jxb/err421>

509 Flavel, R.J., Guppy, C.N., Tighe, M.K., Watt, M., Young, I.M., 2014. Quantifying the

510 response of wheat (*Triticum aestivum* L) root system architecture to phosphorus in an
511 Oxisol. *Plant Soil* 385, 303–310. <https://doi.org/10.1007/s11104-014-2191-9>

512 Furukawa, J., Nakanishi, T.M., Matsubayashi, M., 1999. Neutron radiography of a root
513 growing in soil with vanadium. *Nucl. Instruments Methods Phys. Res. Sect. A Accel.*
514 *Spectrometers, Detect. Assoc. Equip.* 424, 116–121. <https://doi.org/10.1016/S0168->
515 [9002\(98\)01279-0](https://doi.org/10.1016/S0168-9002(98)01279-0)

516 Gewin, V., 2010. An underground revolution. *Nature* 466, 522–533.

517 Grzebisz, W., Floris, W., van Noordwijk, M., 1989. Loss of dry matter and cell contents from
518 fibrous roots of sugar beet due to sampling , storage and washing * 57, 53–57.

519 IPCC, 2007. *Climate Change 2007: The Physical Science Basis*, in: Solomon, S.D., Qin, M.,
520 Manning, M., Chen, Z., Marquis, M., Averyt, K.B., Tignor, M., Miller, H.L. (Eds.),
521 *Contribution of Working Group I to the Fourth Assessment Report of the*
522 *Intergovernmental Panel on Climate Change*. Cambridge,UK and New York, USA.

523 Jenneson, P.M., Gilboy, W.B., Morton, E.J., Luggar, R.D., Gregory, P.J., 1999. Optimisation
524 of X-ray micro-tomography, in: 1999 IEEE Nuclear Science Symposium. Conference
525 Record. 1999 Nuclear Science Symposium and Medical Imaging Conference (Cat.
526 No.99CH37019).

527 Kar, S., Varade, S.B., Ghildyal, B.P., 1979. Pore size distribution and root growth relations of
528 rice in artificially synthesized soils. *Soil Sci.* <https://doi.org/10.1097/00010694->
529 [197912000-00008](https://doi.org/10.1097/00010694-197912000-00008)

530 Keyes, S.D., Daly, K.R., Gostling, N.J., Jones, D.L., Talboys, P., Pinzer, B.R., Boardman, R.,
531 Sinclair, I., Marchant, A., Roose, T., 2013. High resolution synchrotron imaging of
532 wheat root hairs growing in soil and image based modelling of phosphate uptake. *New*

533 Phytol. 198, 1023–1029. <https://doi.org/10.1111/nph.12294>

534 Khoury, C.K., Bjorkman, A.D., Dempewolf, H., Ramirez-Villegas, J., Guarino, L., Jarvis, A.,
535 Rieseberg, L.H., Struik, P.C., 2014. Increasing homogeneity in global food supplies and
536 the implications for food security. *Proc. Natl. Acad. Sci. U. S. A.* 111, 4001–6.
537 <https://doi.org/10.1073/pnas.1313490111>

538 Knox, J., Hess, T., Daccache, A., Wheeler, T., 2012. Climate change impacts on crop
539 productivity in Africa and South Asia. *Environ. Res. Lett.* 7, 34032.
540 <https://doi.org/10.1088/1748-9326/7/3/034032>

541 Kockelmann, W., Zhang, S.Y., Kelleher, J.F., Nightingale, J.B., Burca, G., James, J.A., 2013.
542 IMAT - A new imaging and diffraction instrument at ISIS. *Phys. Procedia* 43, 100–110.
543 <https://doi.org/10.1016/j.phpro.2013.03.013>

544 Koebernick, N., Daly, K.R., Keyes, S.D., George, T.S., Brown, L.K., Raffan, A., Cooper,
545 L.J., Naveed, M., Bengough, A.G., Sinclair, I., Hallett, P.D., Roose, T., 2017. High-
546 resolution synchrotron imaging shows that root hairs influence rhizosphere soil structure
547 formation. *New Phytol.* <https://doi.org/10.1111/nph.14705>

548 Lal, R., 2016. Feeding 11 billion on 0.5 billion hectare of area under cereal crops.
549 <https://doi.org/10.1002/fes3.99>

550 Lynch, J.P., 2007. Roots of the second green revolution. *Aust. J. Bot.* 55, 493–512.
551 <https://doi.org/10.1071/BT06118>

552 Mairhofer, S., Zappala, S., Tracy, S.R., Sturrock, C., Bennett, M., Mooney, S.J., Pridmore,
553 T., 2012. RooTrak: Automated Recovery of Three-Dimensional Plant Root Architecture
554 in Soil from X-Ray Microcomputed Tomography Images Using Visual Tracking. *Plant*
555 *Physiol.* 158, 561–569. <https://doi.org/10.1104/pp.111.186221>

556 Mawodza, T., Brooks, H., Burca, G., Menon, M., 2018. Understanding root architecture and
557 water uptake of water use efficient wheat mutants using neutron and X-Ray CT imaging.
558 STFC ISIS Neutron Muon Source Data J.

559 Menon, M., Robinson, B., Oswald, S.E., Kaestner, A., Abbaspour, K.C., Lehmann, E.,
560 Schulin, R., 2007. Visualization of root growth in heterogeneously contaminated soil
561 using neutron radiography. *Eur. J. Soil Sci.* 58, 802–810. [https://doi.org/10.1111/j.1365-](https://doi.org/10.1111/j.1365-2389.2006.00870.x)
562 [2389.2006.00870.x](https://doi.org/10.1111/j.1365-2389.2006.00870.x)

563 Metzner, R., Eggert, A., van Dusschoten, D., Pflugfelder, D., Gerth, S., Schurr, U., Uhlmann,
564 N., Jahnke, S., 2015. Direct comparison of MRI and X-ray CT technologies for 3D
565 imaging of root systems in soil: potential and challenges for root trait quantification.
566 *Plant Methods*. <https://doi.org/10.1186/s13007-015-0060-z>

567 Mooney, S.J., Morris, C., Berry, P.M., 2006. Visualization and quantification of the effects of
568 cereal root lodging on three-dimensional soil macrostructure using x-ray computed
569 tomography. *Soil Sci.* 171, 706–718.
570 <https://doi.org/10.1097/01.ss.0000228041.03142.d3>

571 Mooney, S.J., Pridmore, T.P., Helliwell, J., Bennett, M.J., 2012. Developing X-ray computed
572 tomography to non-invasively image 3-D root systems architecture in soil. *Plant Soil*
573 352, 1–22. <https://doi.org/10.1007/s11104-011-1039-9>

574 Moradi, A.B., Carminati, A., Vetterlein, D., Vontobel, P., Lehmann, E., Weller, U.,
575 Hopmans, J.W., Vogel, H.-J., Oswald, S.E., 2011. Three-dimensional visualization and
576 quantification of water content in the rhizosphere. *New Phytol.* 192, 653–663.
577 <https://doi.org/10.1111/j.1469-8137.2011.03826.x>

578 Moradi, A.B., Conesa, H.M., Robinson, B., Lehmann, E., Kuehne, G., Kaestner, A., Oswald,
579 S., Schulin, R., 2009. Neutron radiography as a tool for revealing root development in

580 soil: Capabilities and limitations. *Plant Soil* 318, 243–255.
581 <https://doi.org/10.1007/s11104-008-9834-7>

582 Nakanishi, T.M., Matsumoto, S., Kobayashi, H., 1992. Morphological Change of Plant Root
583 Revealed Radiography by Neutron of Tokyo 641, 638–641.

584 Nakanishi, T.M., Okuni, Y., Hayashi, Y., Nishiyama, H., 2005. Water gradient profiles at
585 bean plant roots determined by neutron beam analysis. *J. Radioanal. Nucl. Chem.* 264,
586 313–317. <https://doi.org/10.1007/s10967-005-0713-x>

587 Niu, Y., Jin, G., Li, X., Tang, C., Zhang, Y., Liang, Y., Yu, J., 2015. Phosphorus and
588 magnesium interactively modulate the elongation and directional growth of primary
589 roots in *Arabidopsis thaliana* (L .) *Heynh* 66, 3841–3854.
590 <https://doi.org/10.1093/jxb/erv181>

591 Octopus, 2019. Octopus reconstruction [WWW Document]. URL
592 <https://octopusimaging.eu/octopus/octopus-reconstruction> (accessed 3.1.19).

593 Oswald, S.E., Menon, M., Carminati, A., Vontobel, P., Lehmann, E., Schulin, R., 2008.
594 Quantitative Imaging of Infiltration, Root Growth, and Root Water Uptake via Neutron
595 Radiography. *Vadose Zo. J.* 7, 1035. <https://doi.org/10.2136/vzj2007.0156>

596 Passioura, J.B., Stirzaker, R.J., 1993. Feedforward Responses of Plants to Physically
597 Inhospitable Soil. *Int. Crop Sci. I* 715–719.
598 <https://doi.org/10.2135/1993.internationalcropscience.c114>

599 Pflugfelder, D., Metzner, R., Dusschoten, D. Van, Reichel, R., Jahnke, S., Koller, R., 2017.
600 Non-invasive imaging of plant roots in different soils using magnetic resonance imaging
601 (MRI). *Plant Methods* 1–9. <https://doi.org/10.1186/s13007-017-0252-9>

602 Pierret, A., Moran, C.J., Doussan, C., 2005. Conventional detection methodology is limiting

603 our ability to understand the roles and functions of fine roots. *New Phytol.* 166, 967–
604 980. <https://doi.org/10.1111/j.1469-8137.2005.01389.x>

605 Rich, S.M., Watt, M., 2013. Soil conditions and cereal root system architecture: Review and
606 considerations for linking Darwin and Weaver. *J. Exp. Bot.* 64, 1193–1208.
607 <https://doi.org/10.1093/jxb/ert043>

608 Robinson, B.H., Moradi, A., Lehmann, E., 2008. Neutron Radiography for the Analysis of
609 Plant – Soil Interactions. *Encycl. Anal. Chem. Appl. Theory Instrum.* 1–8.

610 Rudolph-Mohr, N., Vontobel, P., Oswald, S.E., 2014. A multi-imaging approach to study the
611 root-soil interface. *Ann. Bot.* 114, 1779–1787. <https://doi.org/10.1093/aob/mcu200>

612 Sato, E.M., Hijazi, H., Bennett, M.J., Vissenberg, K., Swarup, R., 2015. New insights into
613 root gravitropic signalling. *J. Exp. Bot.* 66, 2155–2165.
614 <https://doi.org/10.1093/jxb/eru515>

615 Senapati, N., Semenov, M.A., 2019. Assessing yield gap in high productive countries by
616 designing wheat ideotypes. *Sci. Rep.* 9, 5516. <https://doi.org/10.1038/s41598-019-40981-0>

617

618 Southon, T.E., Mattsson, A., Jones, R.A., 1992. NMR imaging of roots: effects after root
619 freezing of containerised conifer seedlings. *Physiol. Plant.* 329–334.

620 Stingaciu, L., Schulz, H., Pohlmeier, A., Behnke, S., Zilken, H., Javaux, M., Vereecken, H.,
621 2013. In Situ Root System Architecture Extraction from Magnetic Resonance Imaging
622 for Water Uptake Modeling. *Vadose Zo. J.* 0, 0. <https://doi.org/10.2136/vzj2012.0019>

623 Tötze, C., Kardjilov, N., Manke, I., Oswald, S.E., 2017. Capturing 3D Water Flow in
624 Rooted Soil by Ultra-fast Neutron Tomography. *Sci. Rep.* 7, 6192.
625 <https://doi.org/10.1038/s41598-017-06046-w>

626 Tracy, S.R., Black, C.R., Roberts, J.A., Dodd, I.C., Mooney, S.J., 2015. Using X-ray
627 Computed Tomography to explore the role of abscisic acid in moderating the impact of
628 soil compaction on root system architecture. *Environ. Exp. Bot.* 110, 11–18.
629 <https://doi.org/10.1016/j.envexpbot.2014.09.003>

630 Tracy, S.R., Black, C.R., Roberts, J.A., McNeill, A., Davidson, R., Tester, M., Samec, M.,
631 Korošak, D., Sturrock, C., Mooney, S.J., 2012. Quantifying the effect of soil compaction
632 on three varieties of wheat (*Triticum aestivum* L.) using X-ray Micro Computed
633 Tomography (CT). *Plant Soil* 353, 195–208. <https://doi.org/10.1007/s11104-011-1022-5>

634 Tracy, S.R., Black, C.R., Roberts, J.A., Mooney, S.J., 2013. Exploring the interacting effect
635 of soil texture and bulk density on root system development in tomato (*Solanum*
636 *lycopersicum* L.). *Environ. Exp. Bot.* 91, 38–47.
637 <https://doi.org/10.1016/j.envexpbot.2013.03.003>

638 Tumlinson, L.G., Liu, H., Silk, W.K., Hopmans, J.W., 2008. Thermal Neutron Computed
639 Tomography of Soil Water and Plant Roots. *Soil Sci. Soc. Am. J.* 72, 1234.
640 <https://doi.org/10.2136/sssaj2007.0302>

641 van Noordwijk, M., Floris, J., 1979. Loss of dry weight during washing and storage of root
642 samples. *Plant Soil* 53, 239–240.

643 Vlassenbroeck, J., Masschaele, B., Cnudde, V., Dierick, M., Pieters, K., Van Hoorebeke, L.,
644 Jacobs, P., 2006. Octopus 8: A High Performance Tomographic Reconstruction Package
645 for X-ray Tube and Synchrotron micro-CT, in: *Advances in X-Ray Tomography for*
646 *Geomaterials*. ISTE, London, UK, pp. 167–173.
647 <https://doi.org/10.1002/9780470612187.ch13>

648 Waines, J.G., Ehdaie, B., 2007. Domestication and crop physiology: roots of green-revolution
649 wheat. *Ann. Bot.* 100, 991–8. <https://doi.org/10.1093/aob/mcm180>

650 Wang, M. Ben, Zhang, Q., 2009. Issues in using the WinRHIZO system to determine
651 physical characteristics of plant fine roots. *Shengtai Xuebao/ Acta Ecol. Sin.* 29, 136–
652 138. <https://doi.org/10.1016/j.chnaes.2009.05.007>

653 Warren, J.M., Bilheux, H., Kang, M., Voisin, S., Cheng, C.L., Horita, J., Perfect, E., 2013.
654 Neutron imaging reveals internal plant water dynamics. *Plant Soil* 366, 683–693.
655 <https://doi.org/10.1007/s11104-012-1579-7>

656 Willatt, S.T., Struss, R.G., 1979. Germination and Early Growth of Plants using neutron
657 radiography 415–422.

658 Willatt, S.T., Struss, R.G., Taylor, H.M., 1978. In situ Root Studies Using Neutron
659 Radiography 1–6.

660 Zarebanadkouki, M., Carminati, A., Kaestner, A., Mannes, D., Morgano, M., Peetermans, S.,
661 Lehmann, E., Trtik, P., 2015. On-the-fly Neutron Tomography of Water Transport into
662 Lupine Roots, in: *Physics Procedia*. <https://doi.org/10.1016/j.phpro.2015.07.041>

663 Zarebanadkouki, M., Kim, Y.X., Carminati, A., 2013. Where do roots take up water? Neutron
664 radiography of water flow into the roots of transpiring plants growing in soil. *New*
665 *Phytol.* 199, 1034–1044. <https://doi.org/10.1111/nph.12330>

666 Zarebanadkouki, M., Kim, Y.X., Moradi, A.B., Vogel, H.-J., Kaestner, A., Carminati, A.,
667 2012. Quantification and Modeling of Local Root Water Uptake Using Neutron
668 Radiography and Deuterated Water. *Vadose Zo. J.* 11.
669 <https://doi.org/10.2136/vzj2011.0196>

670